

**TIP OF THE RED GIANT BRANCH DISTANCES TO
GALAXIES:**

11 I. THE DWARF GALAXY SEXTANS A

Shoko Sakai

Jet Propulsion Laboratory, California Institute of Technology, Pasadena, CA 91125

Barry F. Madore

NASA/IPAC Extragalactic Database, Infrared Processing and Analysis Center, California
Institute of Technology, Pasadena, CA 91125

and

Wendy L. Freedman

The Observatories, Carnegie Institution of Washington, Pasadena, CA 91101

Running Headline: *TRGB Distance to Sextans A*

Received _____ accepted --- ----

ABSTRACT

We present color-magnitude diagrams and luminosity functions for stars in the nearby dwarf galaxy Sextans A, based on VI photometry obtained with the COSMIC CCD prime-focus camera on the Palomar 5m telescope. We discuss the previous disagreement in the literature over the zero-point for photometry in Sextans A. The new data presented here shed light on the reasons for these differences and also finally resolve the issue.

The discontinuity of the I -band red giant branch luminosity function has been measured at $I = 21.73 \pm 0.09$ mag. Identifying this feature with the tip of the first-ascent red giant branch at $M_I = -4.01$ mag, gives an independent (Population II) distance modulus estimate of 25.74 ± 0.13 mag (1.42 Mpc) to this galaxy. These data are also used to derive PL relations from the six previously known Cepheids with periods ranging from 10 to 25 days, from which a reddening-corrected true (Population I) distance modulus of 25.85 ± 0.15 mag is derived, corresponding to a linear distance of 1.48 Mpc. The agreement of these two independent distance determinations is extremely encouraging, and together with similar measurements for other nearby galaxies, indicates that the zero points of the Cepheid and TRGB distance scales agree at the 0.1 mag level. Furthermore, it suggests that the TRGB method is of comparable accuracy to the Cepheids.

Subject headings: galaxies: individual - galaxies: dwarf galaxies - galaxies: distances

1. Introduction

To date, the most reliable primary indicator for galaxies is the Cepheid period-luminosity (PL) relation. Hence, the Cepheid PL relation currently forms the basis for the calibration of a wide range of secondary distance indicators, applicable at greater distances than the Cepheids themselves. Given the critical role of the Cepheid distance scale, it is therefore important to measure the distances to nearby galaxies using completely independent techniques both to determine the external error of the Cepheid distance scale, as well as to search for potential systematic errors. Moreover, Cepheid observations are restricted to Population I stars, found exclusively in late type galaxies. An excellent alternative is to employ the tip of the red giant branch (TRGB) method. An attractive feature of this method is that it is applicable to all morphological types of galaxies as long as metal-poor red giant Pop II stars are present.

The first-ascent red-giant branch marks the core helium flash of low-mass stars. The low-mass stars evolve along the red-giant phase up to the TRGB, forming a discontinuity in the luminosity function. Theoretically there is a strong basis for expecting such stars to be good distance indicators: the bolometric luminosity at the core helium flash for low-mass stars of the same metallicity varies by only ~ 0.1 mag for an age range of 2 to 15 Gyr (for example, see Iben and Renzini 1983; Figure 7).

In Paper I of this series, Lee *et al.* (1993) devised a quantitative method of detecting the TRGB based using *I*-band data and employing an edge detection filter. They applied this method to several Local Group galaxies, demonstrating the robustness of the *I*-band TRGB method as a distance indicator for nearby resolved galaxies. This method currently applies over a range of metallicities from $2.2 < [Fe/H] < -0.7$ dex. In Paper II, Madore & Freedman (1994) undertook a number of computer simulations and concluded that the TRGB method can be used to derive distances, with a precision comparable to the Cepheid

distances for galaxies out to at least 3 Mpc using ground-based telescopes. In this paper, we apply the TRGB method to Sextans A and compare the derived distance with that measured from multi-wavelength Cepheid observations.

Sextans A is a dwarf irregular galaxy, believed to be located near the edge of the Local Group. It has an unusual overall shape, appearing square in a sky projection, both in the optical and possibly in III (e.g. Huchtmeier *et al.* 1981). Although it is one of the brightest irregular galaxies in the Local Group, there has been no agreement on the distance to Sextans A mainly due to inconsistent photometric data between previous studies. Using a photographic survey, Sandage & Carlson (1982; hereafter SC82) discovered five Cepheids in this dwarf galaxy and measured a distance modulus of 25.8 mag, corresponding to a distance of 1.45 Mpc. Hoessel, Schommer & Danielson (1983; hereafter H83) obtained CCD observations of Sextans A; they used the original Gunn *GRI* filters which were transformed to the standard Johnson system. This study revealed a zero point difference of as much as 0.2 mag between SC82 and H83. Sandage & Carlson (1985; hereafter SC85) later recalibrated their own photometry and found a distance modulus of Sextans A at 26.2 mag, corresponding to a longer distance of 1.74 Mpc. Walker (1987; hereafter W87) then did a careful analysis of H83 and SC85 photometry by comparing the SC85 data with new observations obtained with a CCD using standard Johnson filters. He found that the SC85 *B* magnitudes were still faint by 0.16 mag. Recently, Piotto, Capaccioli & Pellegrini (1994; hereafter P94) studied the Cepheids in Sextans A and in addition, discovered five additional Cepheid candidates. They obtained the extinction-corrected true distance modulus of 25.71 \pm 0.20 which agrees with the original SC82 study. In summary, the distance to Sextans A is still being debated.

In the next section, we discuss the observations made for the analysis presented in this paper. This is followed by Section 3 in which we compare our photometry with previously

published datasets on Sextans A. The distance to Sextans A estimated from both Cepheid observations and from the TRGB is discussed in Sections 4 and 5 respectively. In Chapter 5, we present a modified quantitative method for determining the position of the TRGB, without employing histograms. We conclude with a discussion and summary.

2. Observations

We observed Sextans A using the 5m Hale Telescope at Palomar Observatory 011 April 1, 1995. Using the prime-focus COSMIC camera with 2048² CCD, covering 9.7 arcmin on a side, we obtained *V* and *I* exposures of 300 and 600 seconds, respectively, under photometric conditions. The data were debiased and flatfielded using standard reduction methods.

Stellar photometry was obtained using the point-spread function fitting packages DAOPHOT and ALLSTAR (Stetson 1987). These packages use automatic star finding algorithms and then fit a point spread function as determined from bright, isolated stars in the same field.

In addition to the Palomar data, we analyzed *B* and *V* data for a smaller region of Sextans A, obtained at the Canada France Hawaii 3.6m Telescope in January 1984. DAOPHOT and ALLSTAR were again used for the photometry reduction. *V* magnitudes were calibrated by tying in the photometry of isolated bright stars to the Palomar data.

B data were calibrated using stars identified in the bright star list in SC82; they were then transformed to the W87's system as described below.

3. Comparison with Previous Studies

The resolved stellar populations of Sextans A have been the subject of several studies in the past decade or so. However, as mentioned in the Introduction, the stellar photometry zero point and thus the distance to Sextans A largely remain uncertain. The first published study was based on BV photographic plates taken at Las Campanas and at Palomar by SC82. H83 then used the original Gunn-Thuan GRI filters, which were mapped to Johnson BVI magnitudes using transformation equations given by Hoessel & Melnick (1980).

Even after SC85 recalibrated their data for Sextans A, an offset in zero point of ~ 0.2 mag remained outstanding between the two datasets. W87 contributed bright-star CCD photometry in an effort to reconcile the ensuing debate over linearity and color corrections between the SC82 and H83 studies. He found that for 34 common stars with $B - V < 0.9$, B magnitudes given in SC85 are 0.16 mag fainter. He also found that his magnitudes agreed very well with those of H83 for blue stars; however for red stars, H83 B magnitudes are fainter by about 0.1 mag.

Finally, Aparicio *et al.* (1987; hereafter A87) presented UBV CCD photometry of 2279 stars in Sextans A, providing a third intercomparison of datasets. The comparison between SC85 and A87 shows a discrepancy of about 1.55 mag in B and 1.45 in V , the former being fainter; the comparison between H83 and A87 gives a zero point difference of ~ 0.13 and 0.16 mag in B and V respectively, which A87 describe as being due to inaccurate photometry transformation from Gunn to Johnson systems in H83. P94 recently published the observations of Cepheid variables in $BVRI$: the comparison of their photometry with others show a very good agreement with W87's data.

The challenge here is to reconcile these different studies and bring the various Cepheid observations onto a common magnitude scale for distance determination purposes

In this section, we compare our V magnitudes for the brightest stars listed in SC82 with four previously-published studies mentioned above: SC82, H83, W87 and A87.

Unfortunately, there is no comparison with the P94 dataset since the magnitudes were not tabulated in their paper. From here on, we will refer to the data presented in this paper as SMF. In Table 1, we give the Palomar CO SMIC VI photometry for bright stars from SC82's list. The comparison results are summarized in Figure 1 and Table 2. In Figure 1, the differences between the magnitudes from other datasets and from SMF are plotted as a function of SMF magnitude. Positive δV corresponds to SMF being fainter. A solid line in each plot is the zero offset line; for the SC82 comparison, this line is drawn at $\delta V = 0.3$ mag. A dashed line represents the least-squares fit for each comparison. As can be seen in Table 2, the photometry presented in this paper agrees very well with that of W87 and H83; the zero point differences between these datasets are less than 0.1 mag. In Table 2, the zero point offset is calculated with respect to the dataset listed in the column. We note that in Table 3 of H83, they identify their star #633 as the SC82 bright star #13. We believe that the star #630 is a more likely candidate, with a magnitude that matches that of SC82 better. Also in H83, the magnitude of the bright star #59 is significantly different from that presented in all of the other studies; this star is not plotted in Figure 1.

We have also made comparisons of B magnitudes from SC82, A87 and W87. Our photometry is essentially on the same scale as W87's. In Figure 2, we show the difference between A87 and SC82, and between W87 and SC82 as a function of SC82 magnitude. We note that the zero point difference between W87 and SC82 primarily comes from its dependence on color. Figure 3 shows the difference between W87 and SC82 B magnitudes as a function of SC82 $B - V$ color. Although the dispersion is large, bluer stars of $B - V < 0.3$ have a systematically larger zero point offset with respect to redder ones. The solid line represents a least squares fit to the color dependence relation; we adopt this fit later on when combining all the data for the distance determination using the Cepheid variables.

4. Luminosity Function and Color-Magnitude Diagram

In Figure 4, the I-band luminosity function for Sextans A is shown. The open histogram includes all the stars found in Sextans A while the solid histogram only includes those stars with photometry errors less than 0.25 mag. The color magnitude diagram for all the stars matched in V and I is shown in Figure 5. We detect a prominent blue plume which is indicative of a recent star formation. In the red supergiant branch, there is a rather noticeable clump at $V - I \sim 1.4$ and $I \sim 13.75$. This group of stars is not associated with any particular location in or around the galaxy; they are spread out throughout the field.

In general, photometric errors are very roughly correlated with the stellar magnitude: that is, for fainter stars, the errors are larger. In a color-magnitude diagram, error bars can be plotted to indicate the uncertainty at a given magnitude level. However, one problem with such plots is that your eyes are attracted to the region with larger error bars, that is, to the data that are statistically less significant. Here, we present plots which in a sense are a combination of grey-scale presentation and smoothing. Plots of this nature have been published previously for the galaxy M81 by Madore *et al.* (1993). For each magnitude in the CMD, 10 points are randomly generated following a Gaussian distribution of variance that equals error in color in x-axis direction and magnitude error in y. This means that for magnitudes with large photometric errors, 10 random points are distributed over a larger region, making them less prominent. Applying this technique to all of the stars in our CMD, we obtain a 'smoothed' diagram shown in Figure 6. In comparison to Figure 5, the red giant branch at the faint end appears more smeared. But most significantly, the blue and red supergiant branches become much more prominent.

5 The Cepheid Distance

In their photographic survey, SC82 discovered five Cepheids whose periods ranged from 1.0 up to 25 days. Later, P94 announced the discovery of five more Cepheids in Sextans A; three of them have very short periods of around 3 to 4 days. In our Palomar V and I data, we recover all five of the SC82 Cepheids and the brighter three of the P94 Cepheid candidates. Four of the SC82 Cepheids were identified in the CFHT data as well. Furthermore, we identified these Cepheids in the tables of previously published photometry in A87, H83 and W87. A r offset of -0.7 mag was applied to the 1183 I magnitudes. In Table 3, all the newly compiled BVI data for Cepheids in Sextans A are listed. The 1994 Cepheid magnitudes have been previously tabulated and are not included. The Cepheid data are plotted in Figure 7. These figures represent random-phase PL relations; no phase corrections or averaging was applied.

The absolute calibrations adopted for the PL relations are expressed as follows (Madore & Freedman 1991):

$$M_B = 2.43(\pm 0.14)(\log P - 1.00) - 3.50(\pm 0.06)[\pm 0.36] \quad (1)$$

$$M_V = -2.76(\pm 0.11)(\log P - 1.00) - 4.16(\pm 0.05)[\pm 0.27] \quad (2)$$

$$M_R = 2.94(\pm 0.09)(\log P - 1.00) - 4.52(\pm 0.04)[\pm 0.22] \quad (3)$$

$$M_I = -3.06(\pm 0.07)(\log I - 1.00) - 4.87(\pm 0.03)[\pm 0.18] \quad (4)$$

Fixing the slopes to those given in the above equations, the zero point for each PL relation in Figure 7, and thus the apparent distance modulus for each wavelength, was determined by minimizing the *rms* fluctuation. To avoid bias due to observational selection effects and the possible influence of overtone pulsators, we use only those Cepheids with periods longer than 10 days. The variable V24 ($P = 10.1791$ days) in the SC82 list is also omitted, since its position on the PL relation deviates significantly from the mean relation, by approximately 1.0 mag. Hence we are left with six Cepheids, four from SC82 and two

from P94. The adopted solution for each wavelength is superposed on the data. The distance moduli for B , V , R and I are respectively 26.06 ± 0.07 , 26.10 ± 0.08 , 25.92 ± 0.13 and 25.95 ± 0.08 mag. Dotted lines above and below the solid-line solutions indicate the $\pm 2\sigma$ -intrinsic width in the calibrating LMC Cepheid sample. Although few points do lie outside the $\pm 2\sigma$ boundaries, we remind the readers that these are random-phase and not phase averaged magnitudes.

SC82 obtained a B distance modulus of 25.8 mag. We converted their magnitudes to W87's system assuming that Cepheid variables have a mean color of $(B-V) \sim 0.7$ mag (Madore 1985) and from Figure 3, we adopt an average offset of $+0.13$ mag for SC82 B data points, in the sense that the SC82 data were originally measured too bright. Minimizing the dispersion and using the slope given in the LMC PL relation above, we obtain the best-fit distance modulus of 25.52 ± 0.12 mag for the modified SC82 data. This estimate is almost 0.4 mag smaller than the B distance modulus we obtain from CCD data independently calibrated and 011 W87's system. We have no explanation at this point as to why the modified SC82 estimate is significantly lower than our value.

Following the procedure outlined in more detail by Madore and Freedman (1991), a reddening law (Cardelli *et al.* 1989) was fitted to our multi-wavelength BVR apparent distance moduli and extrapolated to $\lambda^{-1} = 0$ to determine the true distance modulus for Sextans A. Using those Cepheids with periods longer than 10 days, we obtain the distance modulus to Sextans A of 25.85 ± 0.15 mag. The determination of the true modulus requires finding the minimum χ^2 solution in the bivariate extinction/modulus plane. Thus the error in the true modulus is functionally dependent on the extinction error. This is illustrated in Figure 9 which shows the χ^2 contours of the adopted solution. The dark solid line corresponds to the 10 error ellipse. We note that in Figure 8, a straight line of zero slope fit (i.e. no extinction) at the distance modulus of as high as 26.02 mag does also fit the

data within the error bars. As observed in Figure 9, this solution is within the correlated 1σ error contour of the solution. Conversely, a solution with $\mu_0 \sim 25.7$ and $B(BV) \sim 0.1$ mag also is also consistent with these data.

6. TRGB Distance

From previous work (Mould & Kristian 1986; Lee, Freedman & Madore 1993; Madore & Freedman 1995) we expect to detect stars achieving the peak luminosity along the first ascent red-giant branch at an absolute I-band magnitude of -4.0 ± 0.1 mag. In the wavelength range defined by the I-band filter ($\sim 8000 \text{ \AA}$), the absolute magnitude (but not the color) of the TRGB reaches minimum dispersion in both age and metallicity (*e.g.*, Lee, Freedman & Madore 1993; Da Costa & Arm androff 1990; Green, Demarque & King 1987). The I-band magnitude of the TRGB therefore provides a stable and luminous Population II extragalactic distance indicator equal in brightness to a 6-day Population I Cepheid, but far more numerous, and also present in galaxies of every Hubble type.

Thus, wherever an old population of stars is resolved (Baade’s ‘red sheet’ in irregulars, the bulges and halos of spirals, and in the main bodies of ellipticals), the TRGB method of distance determination can be applied. The main source of confusion in detecting the TRGB (and dilution of the discontinuity of the RGB luminosity function) can result if a population of luminous asymptotic giant branch stars is also present in the galaxy. This effect is a small added source of noise in pure Pop II systems, but may be a substantial contributor of noise in composite systems with a strong intermediate age component. Applying the method at the largest practical galactocentric radii will help in reducing this intermediate-mass contamination found at luminosities somewhat brighter than those of the TRGB. We illustrate the potential effect of an extended giant branch in our analysis of the data for Sextans A, a dwarf galaxy with an obvious history of continuing (perhaps even

episodic) star formation

We first consider the entire photometric I-band data set covering 9.7 by 9.7 arcmin, centered 011 Sextans A. The photometry formally extends to $I = 26$ mag; however, in the differential luminosity function shown in Figure 4, severe incompleteness occurs at $I = 22$ mag, at which point the counts abruptly turn over and blend into the noise at fainter magnitudes. From this point on, we include in our analysis only those stars with photometric errors less than 0.25 mag.

One approach to extracting the appropriate stellar population from the whole sample is to select those stars with $V - I$ ('0101' larger than a certain value. Another effective technique is to use the spatial information. We can easily begin to increase the signal-to-noise ratio on measuring the TRGB discontinuity by focusing our attention on regions that are *a priori* expected to be dominated by this old population. Accordingly we subdivided the data set into three regions: (1) a circular region 2.4 arcmin in radius centered on the main body of Sextans A encompassing all of the active star-forming regions. This region also includes the high-surface-brightness portion of the galaxy, where crowding, confusion and incompleteness will be most severe. (2) An annular region also centered on the galaxy but extending from 2.4 arcmin to 4.7 arcmin, designed to maximize the halo Population 11 (red sheet) contribution, and (3) the remainder of the frame out to 4.7 arcmin from the galaxy center to the NE corner of the CCD. This outer field likely still contains a few extreme halo members of Sextans A; however, for the purposes of discussion this region is hereafter characterized as 'the field'.

Figures 10a through c show the color-magnitude diagrams for the main body, the halo and the field, respectively. It is important to note that the limiting magnitude will be different in each of these regions: with the photometry of single stars in the main body of the galaxy being limited by crowding and confusion, photometry in the outer annulus

and ‘field’ will more likely reach the (fainter) photon noise limit. Even locally within the main body of the galaxy, regions of active star formation will be more confused and have a brighter magnitude limit than other regions of lower activity.

In a previous application of the TRGB distance method, Lee *et al.* (1993) used histograms to examine the luminosity function and to determine the position of the TRGB. A disadvantage of histograms, however, is that ambiguities arise due to the fact that the solution depends both on the binning width and on the starting point of the histogram. In order to minimize this artificial dependence, in this paper we present a modified method for the TRGB determination. The basic idea is to employ a Gaussian-smoothed luminosity function. The details are presented in the Appendix. Figures 11a through c show the results for the Sextans A regions studied: main body, halo and field. We show the luminosity function for each region; below these the edge detection results are shown. The Field sample is very sparse and the edge detection solution shows nothing other than just noise. Examining the body and halo subsamples, the filtered function peaks at $I = 21.64$ and 21.79 mag respectively. From their computer simulations, Madore & Freedman (1995) quantitatively explored the effects of crowding and the shift of the position of the TRGB to brighter magnitudes. This is indeed what we observe for Sextans A; the magnitude of the TRGB of the body sample is brighter by 0.15 mag. In both halo and body samples, we observe a noticeable bump in the filtered function, at magnitude about 0.25 mag brighter than that of the TRGB. The corresponding feature is seen in the luminosity function as a hump at $I \sim 21.6$; it is due to the AGB population mentioned above, and adds extra noise into the TRGB analysis.

The distance modulus is determined via the relation $(m - A_I)_{TRGB} = I_{TRGB} - M_{I,TRGB}$. The absolute magnitude, $M_{I,TRGB}$ is defined as $M_{I,TRGB} = M_{BOL} - BC_I$ which is dependent on the metallicity. From Da Costa & Armandroff (1990) and Lee *et al.* (1993), we have

$M_{BOL} = -0.19[Fe/H] - 3.81$ and $BC_I = 0.881 - 0.243(V - I)_{TRGB}$. This calibration is based on a relation between metallicity and magnitude for RR Lyrae stars of the form $M_V(RR) - 0.17[Fe/H] - 0.82$. The metallicity is expressed in terms of $(V - I)$ color as $[Fe/H] = -12.65 + 12.6(V - I)_{-3.5} - 3.3(V - I)_{-3.5}^2$, where $(V - I)_{-3.5}$ is measured at the absolute magnitude of -3.5 . In order to determine $M_{I,TRGB}$ accurately, we need to iteratively calculate the distance modulus and the metallicity until they converge. For our Sextans A data, the photometry is reasonable, errors reaching approximately 0.1 mag at $I = 22.0$ mag. The most uncertain parameter of course is the metallicity. However, as Lee *et al.* (1993) report, $M_{I,TRGB}$ changes very little as the metallicity varies. Furthermore, at 0.5 magnitude below the TRGB (roughly corresponding to $M_I = -3.5$), the $(V - I)$ color changes very little as a function of I magnitude. For this reason, instead of explicitly calculating the metallicity for Sextans A, we adopt the $(V - I)_{-3.5}$ color of 1.3.

An issue we need to address here is the reddening correction. From the multi-wavelength Cepheid observations, we determined in Section 5 an extinction of $E(B - V) = 0.05 \pm 0.05$. This value, however, is derived for the main body of the galaxy that is dominated by the Population I stars. For the Population II red giant branch found in the halo, we need to make an estimate of reddening. The B -band Galactic extinction in the direction of Sextans A is $A_B = 0.06$ mag (Burstein & Heiles 1984). Using prescriptions of Cardelli *et al.* (1989), we obtain the Galactic extinction in I of $A_I = 0.46A_B = 0.03$ mag, which will be used as the lower limit for the extinction of the Sextans A red giants. For the upper limit, we use $E(B - V) = 0.10 \pm 0.10$ from the Cepheid results, which translates into the extinction value of $A_I = 0.10$. Thus, we adopt the I -band extinction of 0.06 ± 0.06 mag.

Observing Figure 11) and applying the extinction to the TRGB, we obtain $I_{TRGB} = 21.13 \pm 0.09$ mag. The absolute magnitude of the TRGB changes very little as a function of color $(V - I)$. Applying the extinction corrections, we obtain $(V - I) = 1.27$

mag and $M_{I,TRGB} = -4.01 \pm 0.10$ mag. The distance modulus is therefore 25.74 ± 0.13 mag, corresponding to the distance of 1.41 Mpc. This value agrees very well with that derived from the Cepheid observations, 25.85 ± 0.15 mag.

7. Conclusion

We have presented the luminosity function and color-magnitude diagrams for 4486 stars in Sextans A, a dwarf irregular galaxy near to the boundaries of the Local Group, based on *VI* photometry. Six Cepheid variables, with periods ranging from 15 days up to 25 days, were identified in our observations. Combining data from SC82, A87, 1183, W87 and P94, we determined the apparent distance modulus for each wavelength, *BVRI*. Fitting a reddening law we obtain the true distance modulus of 25.85 mag.

We have also independently determined the distance to Sextans A by measuring the position of the tip of the red giant branch. Employing a continuous luminosity function and applying an edge-detection filter as described in the Appendix, we derived a distance modulus of 25.74 ± 0.13 mag, which agrees extremely well with that determined from the Cepheids. These results further confirm the accuracy of the TRGB method as a distance indicator.

8. Acknowledgments

This work was funded in part by grant **** to BFM and by NSF grants AST-87-13889 and AST-91-16496 to WLF. BFM is supported in part by the NASA/IPAC Extragalactic Database (NED) and the Jet Propulsion Laboratory, Caltech. This research has made use of the NASA/IPAC Extragalactic Database (NED) which is operated by the Jet Propulsion Laboratory, Caltech, under contract with the National Aeronautics and Space

Administration. It is a pleasure to thank the staffs of Palomar Observatory and the Canada-France-Hawaii telescope for their assistance during the observing for this program.

A. Quantitative Determination of the TRGB position

In this Appendix, we present our revised method for obtaining a quantitative estimate for the position of the TRGB. It is an updated version of the histogram method presented in Lee *et al.* (1993). Instead of histograms, we express the 1-band luminosity function by a continuous probability distribution function and operate on that as follows.

First the luminosity function, $\phi(m)$, is determined by replacing the discretely distributed stellar magnitudes by their corresponding Gaussians, following the expression:

$$\Phi(m) = \sum_{i=1}^N \frac{1}{\sqrt{2\pi}\sigma_i} \exp\left[-\frac{(m_i - m)^2}{2\sigma_i^2}\right], \quad (\text{A1})$$

where m_i and σ_i are the magnitude and photometric error of i th star respectively and N is the total number of stars in the sample. It is essentially a sum of normalized Gaussians such that a magnitude with small photometry error gives a more strongly peaked Gaussian.

The discrete Sobel edge detection filter used by Lee *et al.* (1993) employed a kernel of $[-2,-1,0,+1,+2]$. It operates as a localized slope estimator. To apply this filter as a smooth, continuous function, we define the following adaptive edge detection filter:

$$E(m) = \Phi(I + \bar{\sigma}_m) - \Phi(I - \bar{\sigma}_m). \quad (\text{A2})$$

In this continuous version, “the support for the kernel” is defined by the mean local statistical properties of the data, where the variable $\bar{\sigma}_m$ is the m th photometric error for all stars with magnitude between $m - 0.05$ and $m + 0.05$.

The above method, however, oversmooths the distribution function. It applies a Gaussian smoothing on a point-by-point basis when determining the continuous luminosity

function: an additional smoothing is incorporated in the edge detection expression which depends on the mean Gaussian error. To compensate for this effect, we reduced the effective error term in Equation A1 by a factor of two when determining the TRGB position for the results presented in this paper.

REFERENCES

- Aparicio, A., Garcia-Pelayo, J. M., Moles, M. & Melnick, J., 1987, *A&AS*, 71, 297
- Burstein, D. & Heiles, C., 1984, *ApJS*, 54, 33
- Cardelli, J. A., Clayton, G. C. & Mathis, J. S., 1989, *ApJ*, 345, 245
- Da Costa, G. S. & Armandroff, T. E., 1990, *AJ*, 100, 162
- Green, E. M., Demarque, P. & King, C. R., 1987, *The Revised Yale Isochrones and Luminosity Functions* (New Haven: Yale Univ. Obs)
- Hoessel, J. G. & Melnick, J., 1980, *A&A*, 84, 317
- Hoessel, J. G., Schommer, R. A. & Danielson, G. E., 1983, *ApJ*, 274, 577
- Lee, M. G., Freedman, W. I. & Madore, B. F., 1993, *ApJ*, 417, 553
- Madore, B. F., 1986, in *Cepheids: Theory and Observations*, ed. B. F. Madore (Cambridge: Cambridge University Press), p.167
- Madore, R. F. & Freedman, W. I., 1991, *PASP*, 103
- Madore, B. F. & Freedman, W. I., 1995, *AJ*, 109, 1645
- Madore, B. F., Freedman, W. I. & Lee, M. G., 1993, *AJ*, 104, 2243
- Mould, J. & Kristian, J., 1986, *ApJ*, 305, 591
- Piotto, G., Capaccioli, M. & Pellegrini, C., 1994, *A&A*, 287, 371
- Sandage, A. & Carlson, G., 1982, *ApJ*, 258, 439
- Sandage, A. & Carlson, G., 1985, *AJ*, 90, 1019

Stetson, P. B., 1987, *PASP*, 99, 191

Walker, A. R., 1987, *MNRAS*, 224, 935

Wand, M. P. & Jones, M. C., 1995, "Kernel Smoothing", Chapman & Hall: London

Figure Captions

Fig. 1 - Comparison of V magnitudes of bright stars in Sextans A. The solid line in each graph represents the zero-point level, except in the case of SC82 comparison, this line is offset by +0.3 msg. The dashed lines represent the least-squares fits.

Fig. 2 - Comparison of B magnitudes of bright stars. In top figure, A87 and W87 magnitudes are compared against the SC82 data. The bottom figure shows the difference between W87 and A87 magnitudes as a function of W87.

Fig. 3 - The difference between W87 and SC82 B magnitudes as a function of $B - V$ color. The solid line represents the least-squares fit.

Fig. 4 - The I -band luminosity function of stars in Sextans A. The open histogram shows all the stars found by DAOPHOT. The solid histogram consists only of those with photometry error less than 0.25 msg.

Fig. 5 -1 - $(V - I)$ color-magnitude diagram for 4486 stars in Sextans A.

Fig. 6 - Same as Figure 5 except that 10 random points are generated for each magnitude (see text).

Fig. 7 - PI-relation for six Cepheid variables in Sextans A in B , V , R and I . The solid line in each figure represents the PI relation for each wavelength that minimizes the dispersion. Dotted-lines above and below signify $3\text{-}\sigma$ errors in the LMC calibration of the PI relations.

Fig. 8 - The multi-wavelength fit of reddening to $BVR I$ apparent distance moduli for Sextans A. We obtain the true distance modulus of 25.85 msg.

Fig. 9 - A contour plot showing the chi-square values from fits in determining the true distance modulus. The bold line represents the 1σ contour.

Fig. 10-1 - $(V - I)$ color-magnitude diagrams for the (a) main body of the Sextans A, within 2.4 arcmin from the center, (b) halo which is defined as an annulus extending from 2.4 to 4.7 arcmin and (c) field region, the remainder of the frame.

Fig. 11 - I -band luminosity functions (*top*) and results after applying the edge-detection filter for three subregions of Sextans A. The tip of the red giant branch is detected at $I = 22.79$.

Table 1: Palomar COSMIC VI Photometry of
SC82 Bright Star Sample in Sextans A

No.	V	σ_V	I	σ_I	No.	V	I	σ_I
3	20.024	0.017	19.827	0.028	36	19.632	19.546	0.028
4	18.761	0.015	18.527	0.031	37	19.770	18.257	0.025
5	19.396	0.016	19.189	0.027	38	19.247	19.114	0.027
6	20.095	0.019	20.141	0.033	39	18.607	17.254	0.025
7	18.931	0.015	18.579	0.025	40	20.636	19.169	0.026
8	19.963	0.017	19.863	0.033	41	19.966	18.390	0.025
9	19.554	0.016	18.077	0.025	42	19.712	19.456	0.027
10	19.821	0.017	19.768	0.030	43	20.500	19.115	0.025
11	19.990	0.018	19.865	0.030	44	20.057	20.013	0.033
12	18.783	0.015	18.511	0.025	45	20.236	18.760	0.025
13	19.339	0.016	19.003	0.025	46	19.849	18.380	0.025
14	19.395	0.016	19.191	0.020	47	19.556	19.360	0.027
15	17.525	0.015	17.149	0.027	48	19.556	19.376	0.027
16	20.290	0.018	18.785	0.026	49	19.743	19.073	0.025
17	19.272	0.016	19.165	0.027	50	18.455	16.784	0.081
18	20.017	0.018	18.375	0.025	51	19.535	19.573	0.027
19	19.706	0.015	19.829	0.035	52	18.549	18.353	0.025
20	20.006	0.017	20.126	0.039	53	19.094	19.148	0.026
22	20.125	0.018	18.778	0.026	54	19.810	19.930	0.031
23	20.345	0.020	20.344	0.034	55	19.976	20.052	0.032
24	19.938	0.018	19.712	0.032	56	18.600	16.988	0.136
25	20.240	0.017	20.267	0.035	57	19.330	17.818	0.024
26	19.961	0.016	19.929	0.030	58	19.721	18.148	0.026
27	20.324	0.018	18.782	0.025	59	19.560	19.403	0.026
29	19.253	0.016	18.884	0.025	60	20.084	20.232	0.036
30	19.592	0.016	19.285	0.029	61	19.628	19.312	0.026
31	19.637	0.016	19.704	0.030	63	19.389	19.421	0.027
32	19.458	0.016	19.160	0.026	65	19.825	18.273	0.025
33	19.507	0.015	19.197	0.027	66	18.807	18.099	0.025
34	19.916	0.018	19.715	0.031	67	20.175	20.028	0.033
35	18.243	0.015	17.342	0.025	69	20.228	19.968	0.031

Table 2a Photometry Comparisons: Zero Point Differences

	W87	SC82	A87	1183
This Paper	-0.009	-0.289	-0.108	40.002
W87		-0.274	-0.119	4-0.010,
SC82			+0.161	+0.253
A87				+0.115

Table 2b: Photometry Comparisons: Standard Deviations

	W87	SC82	A87	1183
This Paper	0.083	0.133	0.115	0.094
W87		0.140	0.105	0.113
SC82			0.160	0.168
A87				0.115

Table 3: The Cepheids in Sextans A

Source/JD	Cepheid	Period	B	σ_B	V	σ_V	I	σ_I
Palomar 2449809.7	V I	15.5522	21.14	0.03	20.44	0.10
	V 3	21.2115	20.40	0.02	19.60	0.03
	V24	10.1791	21.47	0.03	20.81	0.04
	V25	18.5590	21.12	0.03	20.18	0.03
	V28	25.4370	21.02	0.03	19.98	0.04
CFHT 2445790.1	V 1	15.552 2	21.76	0.15
	V 3	21.2115	21.77	0.13	20.94	0.12
	V25	18.5590	22.39	0.14	22.02	0.18
	V28	25.4370	20.57	0.11
A87 ¹	V 3	21.2115	20.48	0.04	21.03	0.06
	V24	10.1791	21.18	0.06	21.64	0.10
	V25	18.5590	21.36	0.13	22.15	0.13
	V28	25.4370	20.84	0.03	21.64	0.06
HSM ²	V 3	21.2115	21.88	0.14	20.96	0.10	20.69	0.09
	V24	10.1791	21.41	0.07	21.16	0.12	21.25	0.14
	V28	25.4370	22.02	0.17	21.26	0.05	20.90	0.08
W87 ³	V25	18.5590	22.47	...	21.74
	V28	25.4370	22.02	...	20.90

¹Observed during February 25-27, 1985. ²Observed in May 1981. ³Observed on February 14, 1986.

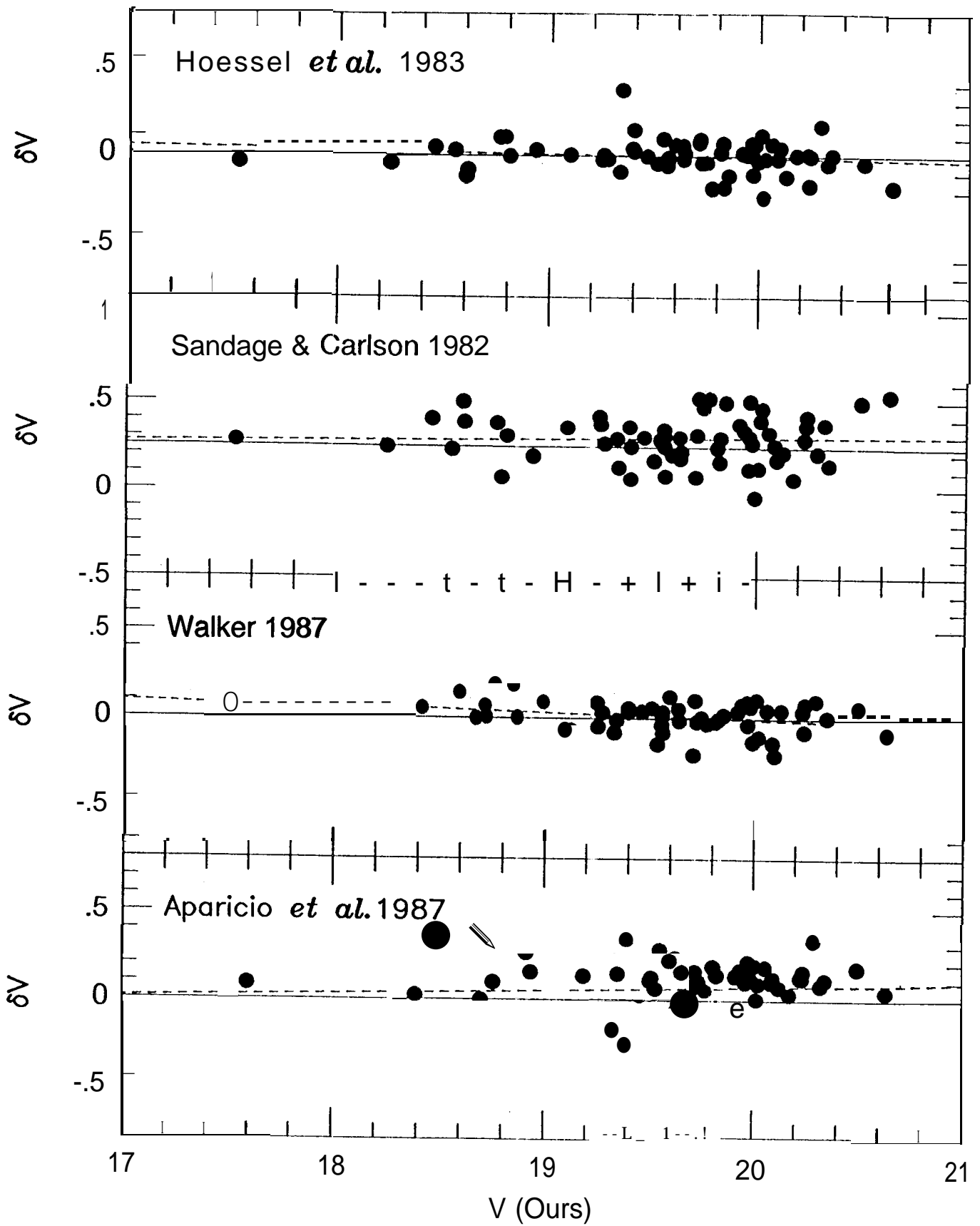
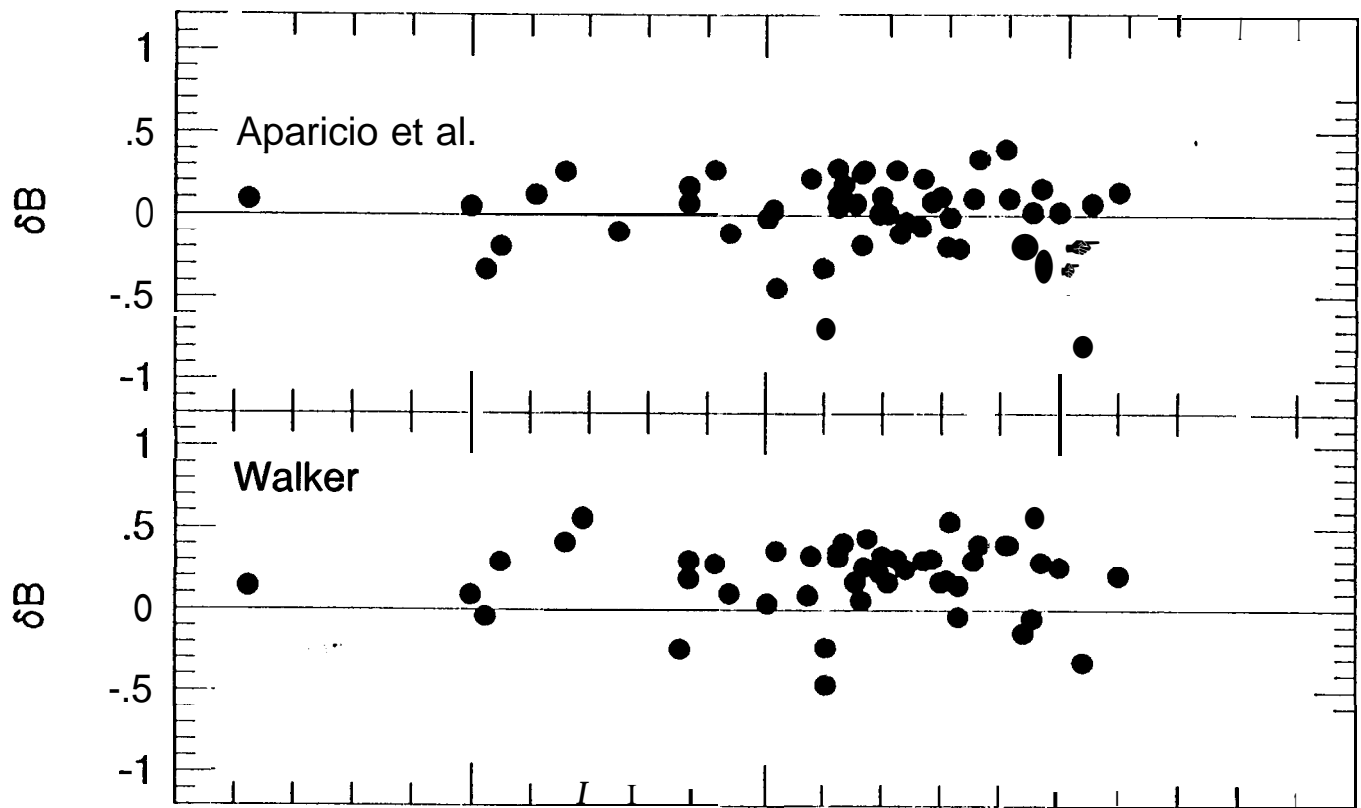


FIG 7



SC82

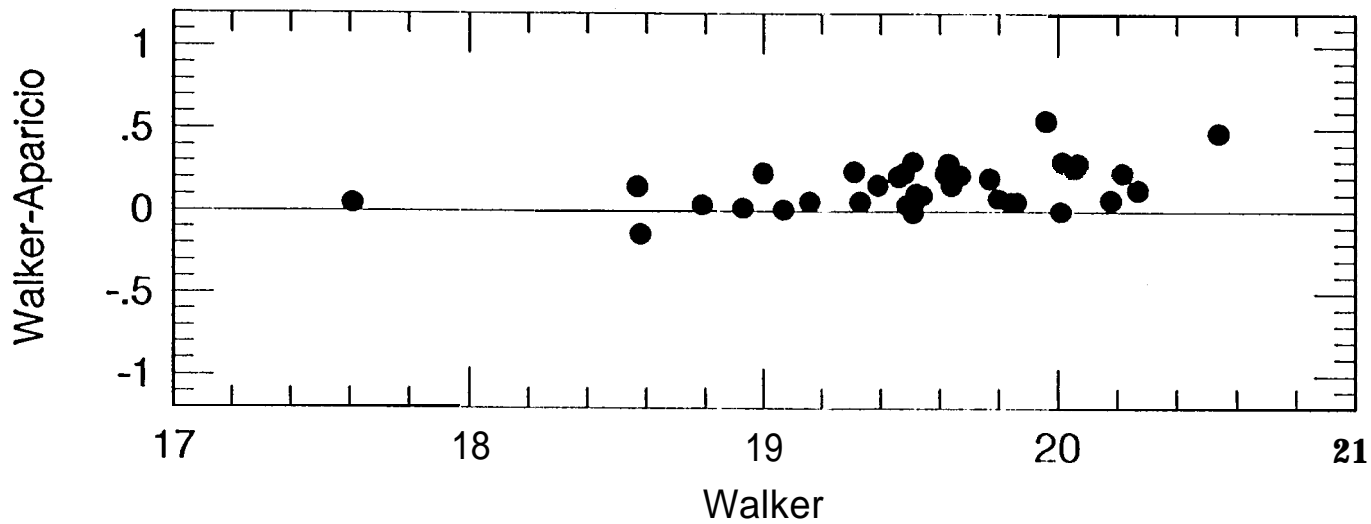
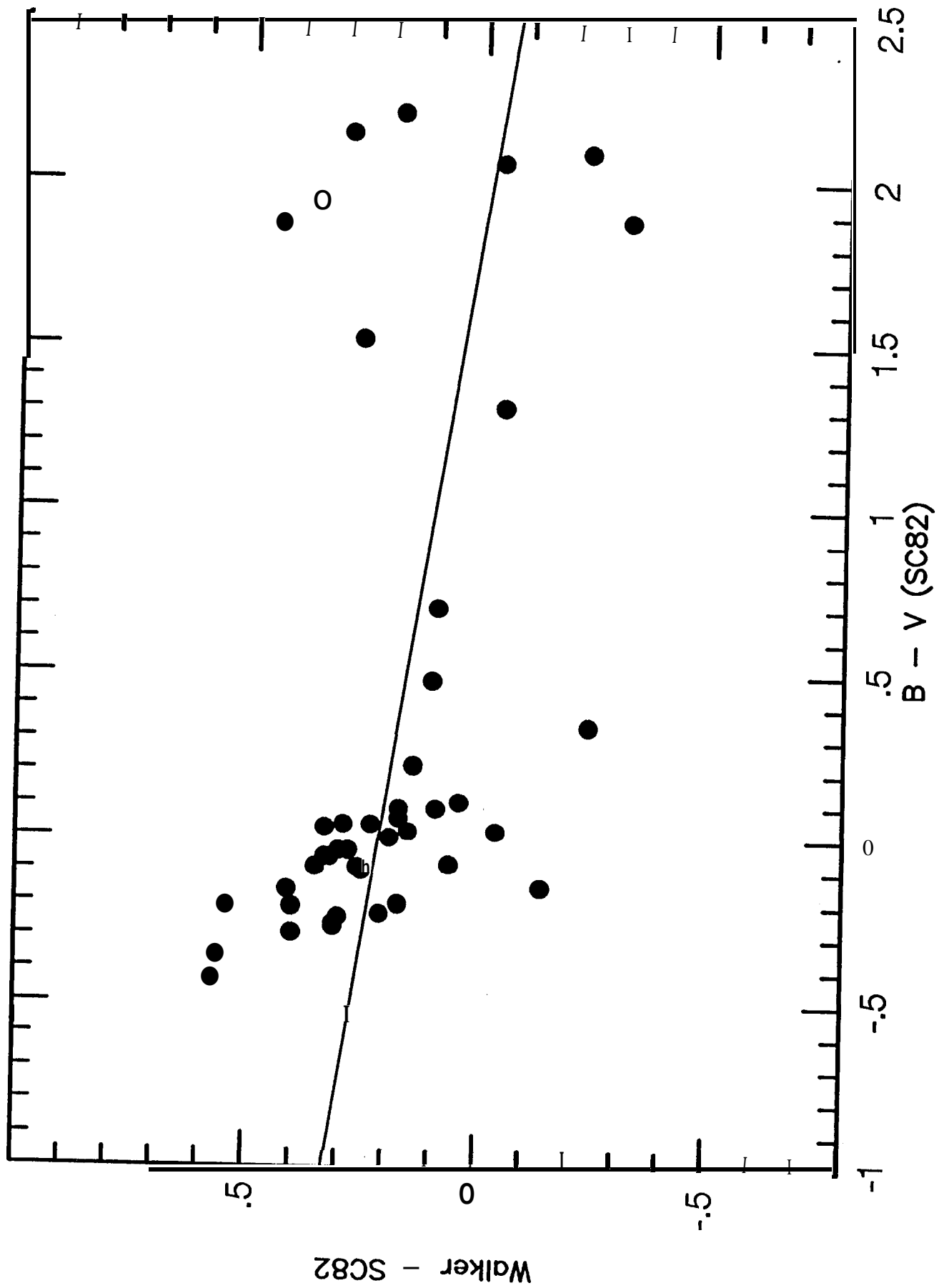
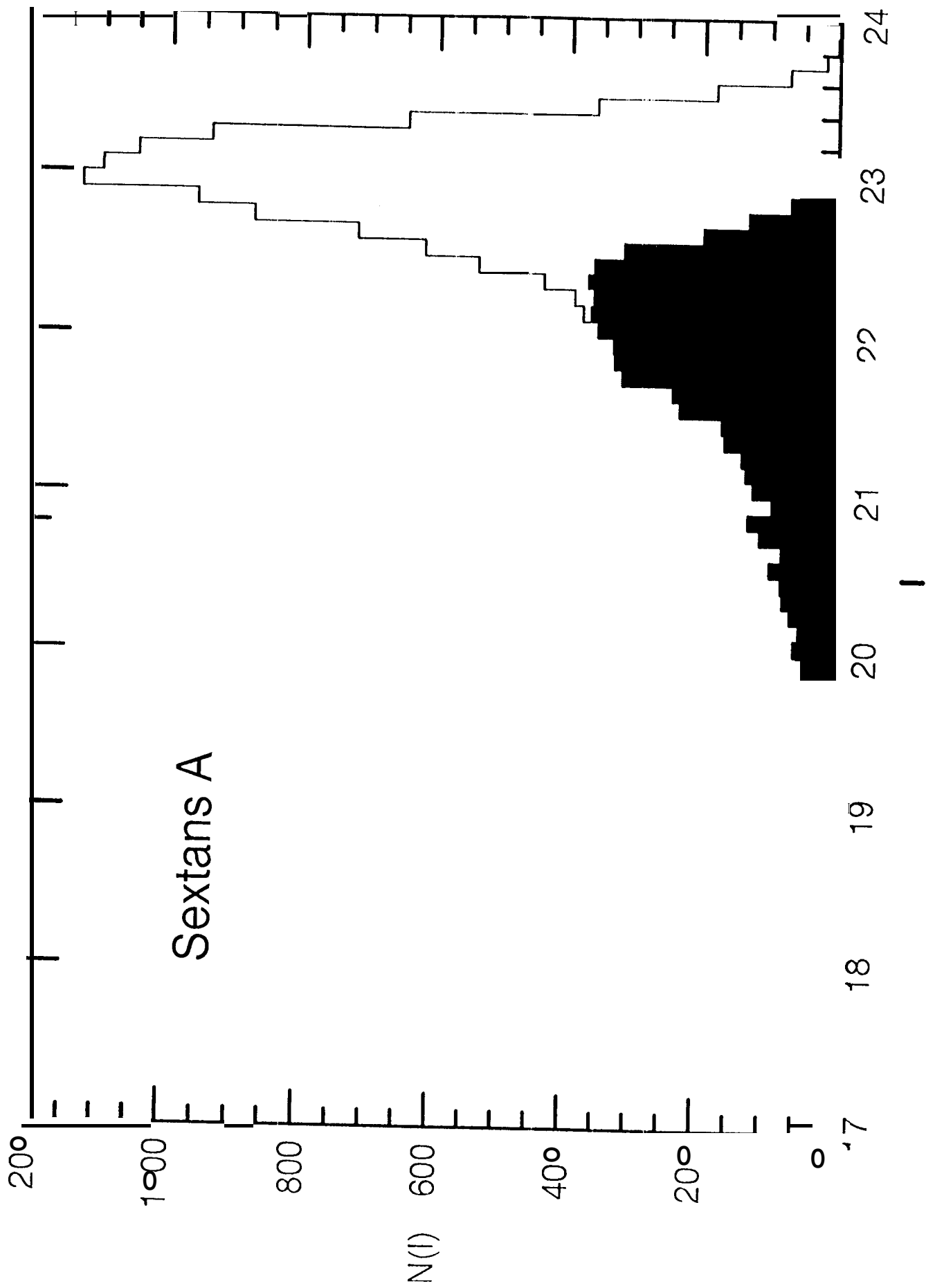
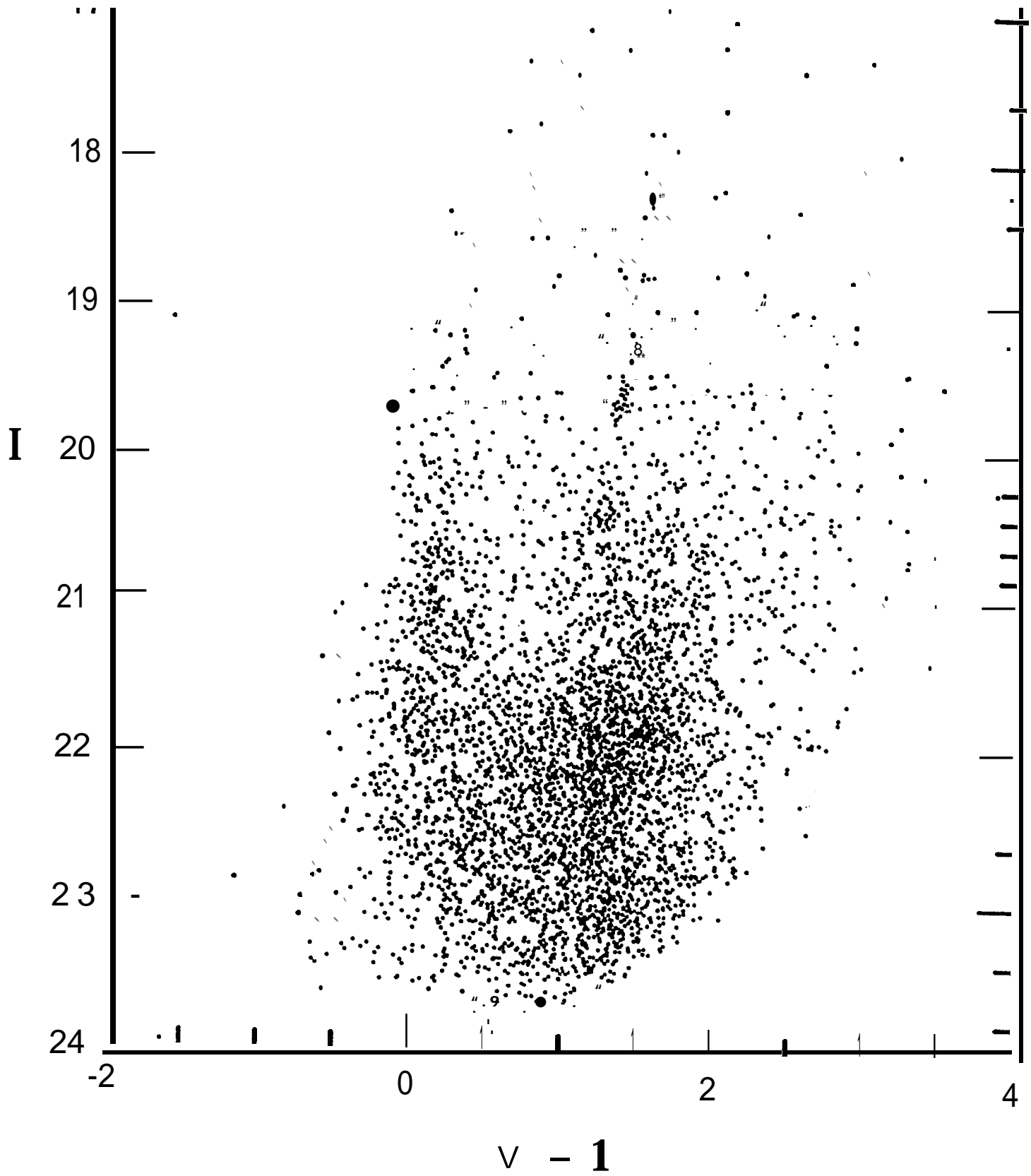
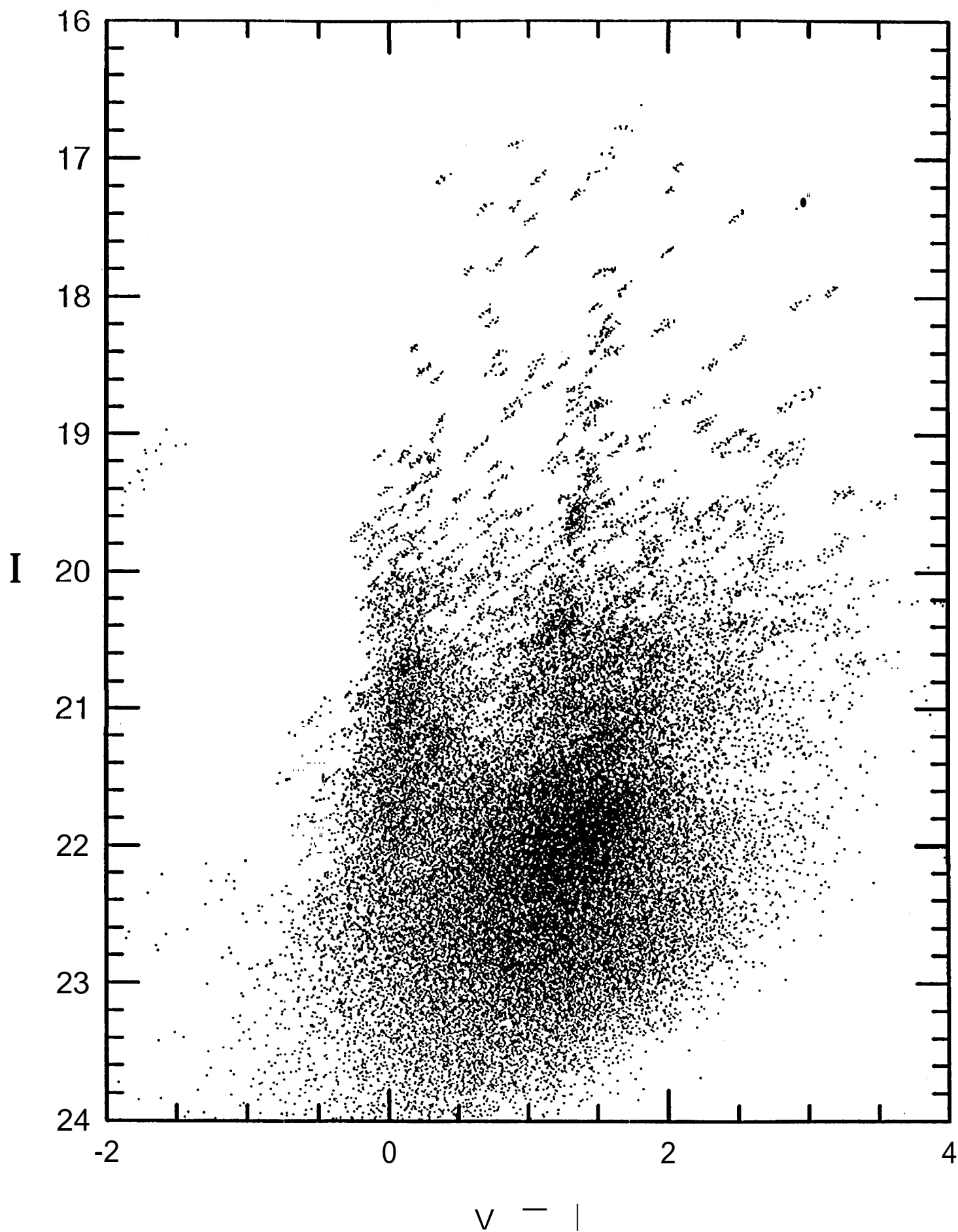


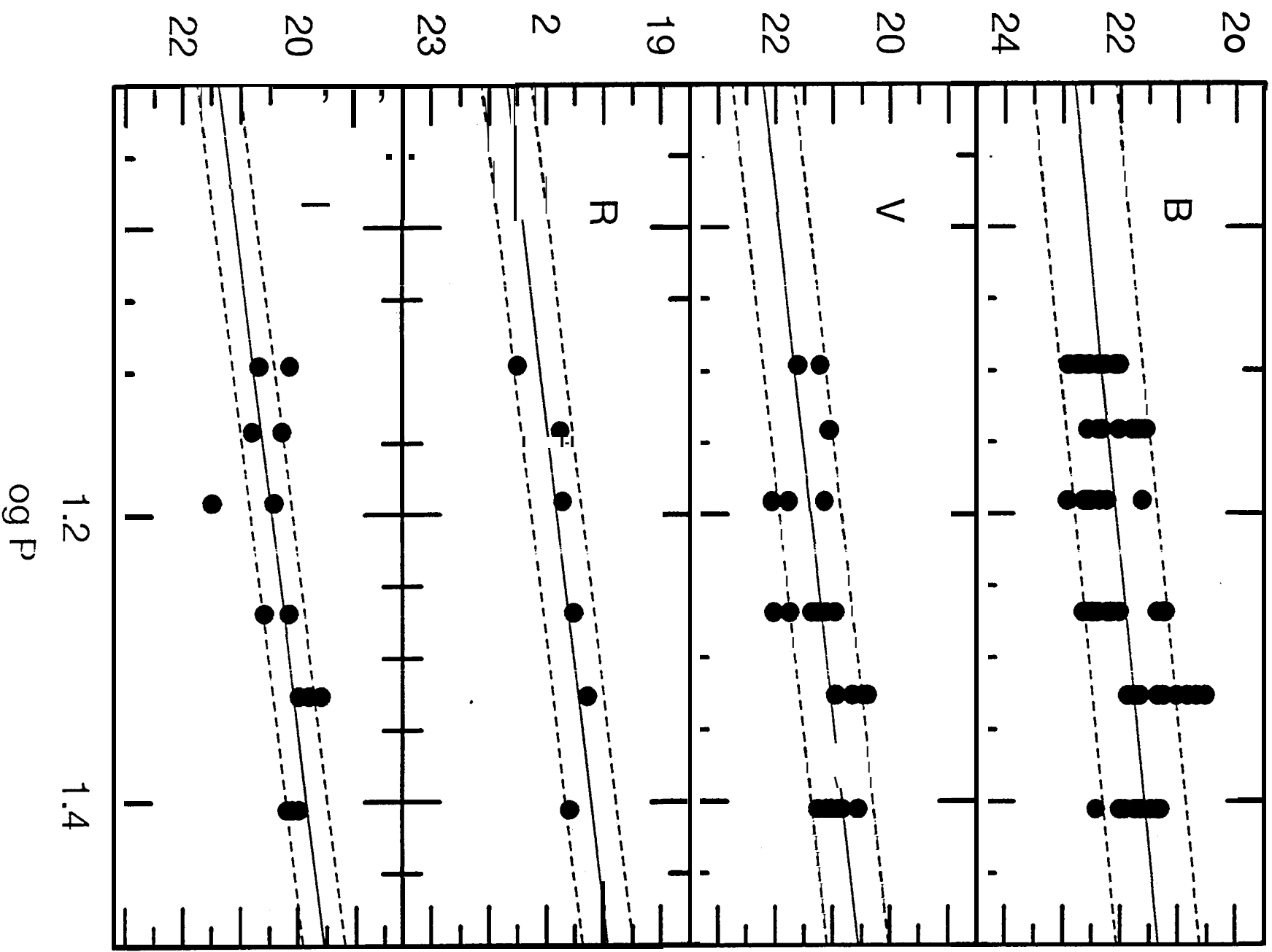
FIG 3



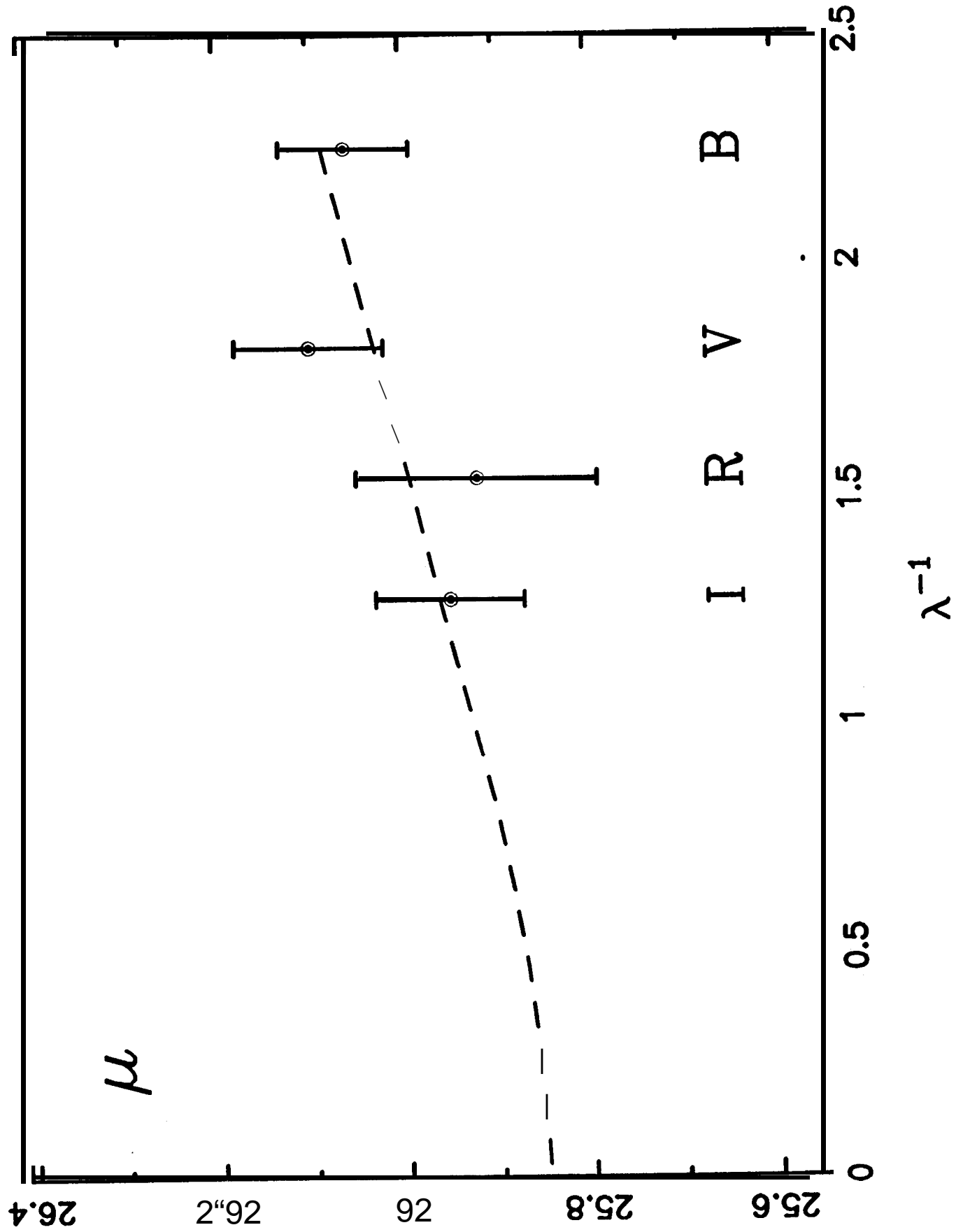








Sextans A



Chi-Squared Surface

